ULTRASONIC DEPASSIVATION IN THE ELECTROCHEMICAL-ULTRASONIC HYBRID MACHINING

Liviu-Daniel Ghiculescu[1], Cornel-Cristian Enciu[1], Ovidiu-Dorin Alupei-Cojocariu[1], Marius-Vali Lazăr[1]
[1]POLITEHNICA University of Bucharest, cornel.enciu@upb.ro, daniel.ghiculescu@upb.ro, cojocariu.alupei@upb.ro, marius_vali.lazar@upb.ro

ABSTRACT: The paper deals with the presentation of the methods for depassivating the iron hydroxide layer in electrochemical-ultrasonic hybrid machining. Ultrasonic depassivation, specific to the electrochemical-ultrasonic hybrid machining, was studied using the specialized software Comsol Multiphysics, focusing on the removal of the passivated iron oxide layer through the action of ultrasonic cavitation induced in the machining working gap. Before defining the parameters in Comsol Multiphysics to build the geometry of the elements needed for modeling and simulation, the shear fatigue resistance of iron oxide and the implosion time of cavitation bubbles were calculated using Rayleigh's equation. An experimental equipment was constructed to test and validate the research carried out with the aid of specialized software tools.
KEYWORDS: electrochemical machining, ultrasound, depassivation, simulation, modeling.

1. INTRODUCTION

Electrochemical Machining (ECM) of a surface takes place within an electrolytic cell, and the underlying phenomenon is anodic dissolution, allowing controlled removal of electrically conductive material. In this process, the tool acts as the cathode, while the surface to be machined serves as the anode, both immersed in an electrolyte solution, which may be a base, acid, or salt. Primarily, the electrolyte fluid must flow between the tool and the work surface, and through the potential difference between them, a direct current is generated in the machining working gap, resulting in the electrolysis phenomenon [1,2].
In the polishing or finishing of surfaces by ECM, the anodic dissolution phenomenon, which occurs in the electrolytic environment due to the high-intensity electric field created between the tool (cathode) and the workpiece (anode), can be explained as follows: a passivated layer forms on the surface of the workpiece, with a thinner thickness in the region of micro-peaks [3]. It follows that the electrical resistance is lower in these areas on the surface of the workpiece. Moreover, the intensity is higher in the micro-peak regions. Therefore, metal particle dissolution begins first in these areas (where the current density is highest) and gradually progresses toward the bottom of the micro-depressions until the entire surface is affected. This implies a critical time at which machining should be stopped, allowing only the micro-peaks to be removed [4].

The removal of the passivated layer is facilitated by applying ultrasound in a hybrid technology alongside electrochemical machining, through the action of ultrasonic cavitation.

For better results in the electrochemical-ultrasonic hybrid finishing of high-alloy steels, acid-based electrolytes can also be used, though they are more costly and highly toxic [5,6]. Another option would be to use electrolyte solutions based on salts (NaCl, NaNO3) that are less expensive and easier to handle.

2. DEPASSIVATION METHODS

According to the schematic in figure 1, there are multiple solutions for removing the neutral, passivated layer that forms on the processed surface during ECM.

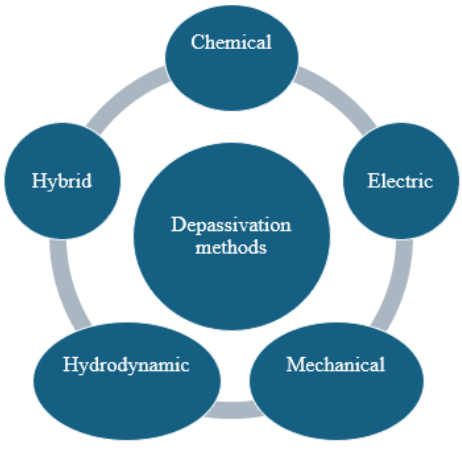

Figure 1. Depassivation methods - the author's contribution based on the information in [7,10]

The technical solutions include: introducing substances (ions) into the electrolyte that react with the ions in the passivated layer - chemical depassivation; using pulsed current machining, which undermines the passivated layer, and reversing polarity during pause time - electrical depassivation;

the mechanical action of abrasive particles in the electrolyte - mechanical depassivation; removal of the passivated layer by electrolyte introduced at high pressure (over 2 MPa) into the machining working gap - hydrodynamic depassivation; and layer removal through electric discharges or ultrasonic cavitation - hybrid depassivation.

The main depassivation methods are presented in detail as follows:

a. Chemical depassivation involves introducing ions into the electrolyte that react with those in the passivated layer, leading to its dissolution.

A potential disadvantage is the alteration of electrical conductivity and, consequently, the current (current density), which affects the material removal process.

b. Electrical depassivation is achieved by using current pulses; the depassivated layer that forms is reduced because it occurs only during the duration of the pulses. During the pause period, the electrolyte removes the formed passivated layer.

Additionally, during the pause, the polarity is reversed, making the workpiece the cathode, where H_2 can form. The release of H_2 also contributes to the removal of the passivated layer (figure 2).

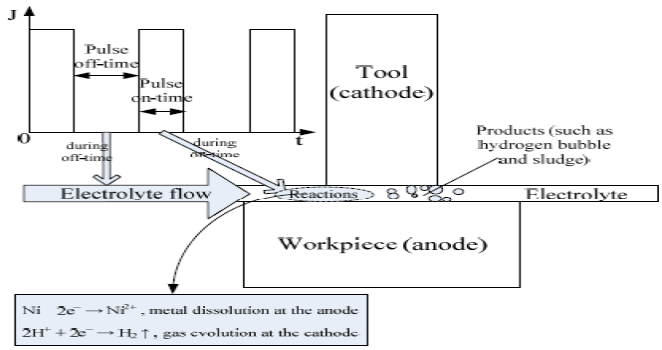

Figure 2. Electrical depassivation mechanism [4,7]

c. Hydrodynamic depassivation is achieved using high pressure of the electrolyte (over 2 MPa) introduced into the machining working gap.

d. Hybrid depassivation is specific to hybrid technologies and can be achieved in several ways: electric discharges in the electrolyte (ECDM); cavitation produced by ultrasound (ECM+US).

In this case, elements from two technological systems, ECM and EDM, are coupled.

The coupling of two components within a hybrid machining process increases costs, but these can be offset by enhanced technological performance, specifically productivity parameters (effective depassivation) and the quality of the processed surface.

3. MODELING OF ULTRASONIC DEPASSIVATION

In the Comsol Multiphysics software, by successively accessing: 2D, Structural Mechanics, Solid Mechanics, Time Dependent, the following case was defined:

- Modeling the depassivation of the iron oxide layer formed on the processed surface of C120 steel, considering a pressure in the range of tens of MPa produced by ultrasonic-induced cavitation in the machining working gap.

Reactions

- $NaCl = Na^+ + Cl^-$ (the dissociation of sodium chloride into chloride and sodium ions)
- $Fe + 2Cl = FeCl_2$ (the reaction of chlorine ions with iron → intermediate salt)
- $2Na + 2H_2O = 2NaOH + H_2 \uparrow$ (the reaction of sodium ions with water at the cathode)
- $FeCl_2 + 2NaOH = 2NaCl + Fe(OH)_2 \downarrow$ (the reaction of iron chloride with sodium hydroxide, resulting in the regeneration of sodium chloride)
- $4Fe(OH)_2 + 2H_2O + O_2 = 4Fe(OH)_3$ (the reaction of iron hydroxide with water and oxygen from the environment → formation of the precipitate)

The working parameters are presented in figure 3.

Parameters

Name	Expression	Value	Description
hp	5[mm]	0.005 m	part height
lp	10[mm]	0.01 m	part width
Ra	1.6e-6	1.6E-6	roughness before ECM+US
PRa	0.1[mm]	1.0E-4 m	the pitch of micro-irregularities
acr	4e-6	4.0E-6	microdepression radius before ECM+US
bcr	3.6e-6	3.6E-6	microdepression depth before ECM+US
pf	0.5e-6	5.0E-7	passivated film thickness at the top of the microgeometry
tus	64.7e-6	6.47E-5	cavitation bubble implosion time
modulC120	200[GPa]	2.0E11 Pa	Young's modulus C120
nuPC120	0.3	0.3	Poisson's ratio in steel C120
tau0	336	336	breaking strength shear fatigue [MPa] C120
pus	17[MPa]	1.7E7 Pa	cavitation US pressure
modulFe2O3	300[GPa]	3.0E11 Pa	iron oxide Young's modulus
roFe2O3	4345	4345	iron oxide density
nuPFe2O3	0.24	0.24	Poisson's ratio to iron oxide
tau0Fe2O3	57.6	57.6	breaking strength shear fatigue [MPa] iron oxide
Rz	4*Ra	6.4E-6	the maximum height of the micro-irregularities

Figure 3. Working parameters

The shear fatigue strength of iron oxide (τ_0) was determined using the equation [8]:

$$\tau_0 = 0{,}6 \cdot 1{,}6 \cdot \sigma_r \quad [\text{MPa}] \quad (1)$$

$$\tau_0 = 0{,}6 \cdot 1{,}6 \cdot 60 = 57{,}6 \text{ MPa}$$

where σ_r is the static breaking strength.

The implosion time of the cavitation bubbles (tus) was calculated based on Rayleigh's equation [9]:

$$\tau = 0{,}915 R_m \sqrt{\frac{\rho}{p_h}} \quad [s] \quad (2)$$

where τ is the implosion time of the cavitation bubbles [s], R_m is the working gap [m]; ρ is the density of the electrolyte (5% NaCl) [kg/m³], and p_h is the hydrostatic pressure [Pa].

Before analyzing the simulation results in the Study - Time Dependent menu, the gas bubble implosion time was defined, as shown in figure 4.

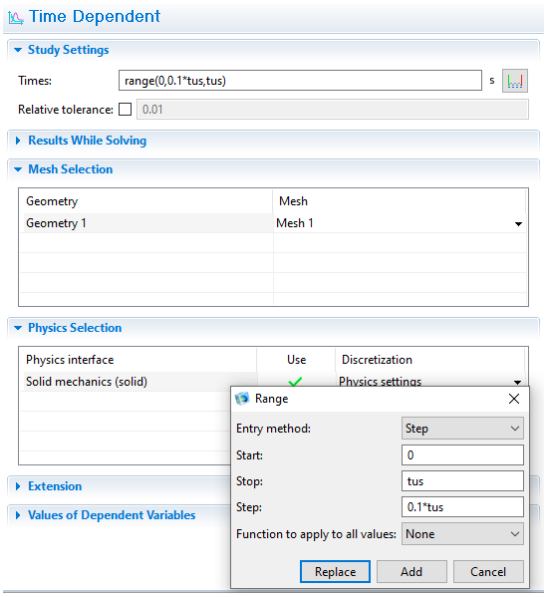

Figure 4. Defining the parameter tus

By substituting the parameter values, R_m = 0,0007 [m] (considering $R_m = s_F$), ρ = 1034 [kg/m³], and p_h = 101325 [Pa] (assuming it is equal to atmospheric pressure), it results in τ = tus = 64,7 µs = 0,0000647 s.

The geometry of the base material is created using geometric functions such as Rectangle, Point, Ellipse, and Square, defined by the parameters in figure 3, along with Boolean operations like Difference.

After defining the geometry of the base material, the materials were applied to each element as follows: C120 steel as the base material, and iron oxide for the microgeometry peaks or the passivated layer.

The characteristics of these materials are presented in figures 5 and 6.

Material Contents

	Property	Name	Value	Unit	Property group
✓	Density	rho	rho(T[1/K])[kg/m^3]	kg/m^3	Basic
✓	Young's modulus	E	modulC120	Pa	Basic
✓	Poisson's ratio	nu	nuPC120	1	Basic

Figure 5. Basic characteristics of C120 steel (D3) [10]

Material Contents

	Property	Name	Value	Unit	Property group
✓	Density	rho	roFe2O3	kg/m^3	Basic
✓	Young's modulus	E	modulFe2O3	Pa	Basic
✓	Poisson's ratio	nu	nuPFe2O3	1	Basic

Figure 6. Basic characteristics of iron oxide [10]

Figures 7 and 8 highlight the area of application of ultrasonic cavitation pressure and the system for orienting and securing the workpiece.

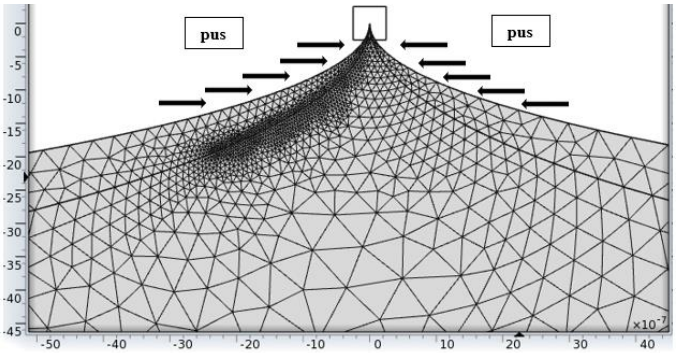

Figure 7. Area of application of ultrasonic cavitation pressure

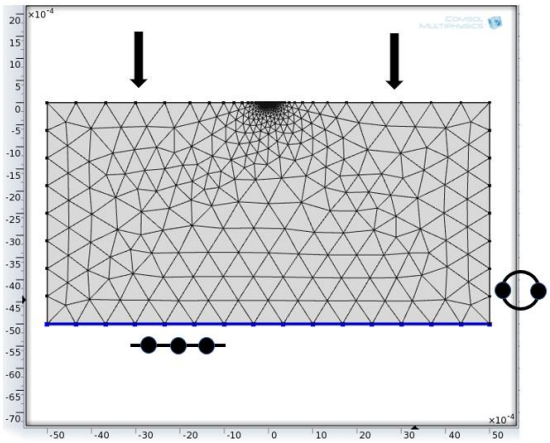

Figure 8. The system for orienting and fixing the workpiece

In figure 9, it can be observed that the highest precision is concentrated near the origin of the workpiece, where the actual removal of the passivated layer occurs, with the greatest connectivity at the peaks of the microgeometry. The results of the statistic for the model are presented in figure 10.

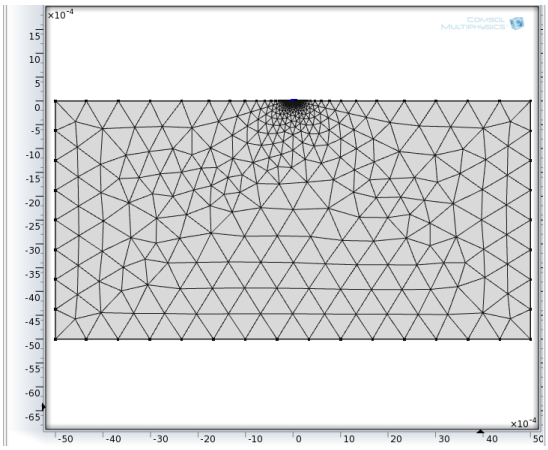

Figure 9. Discretization of the model

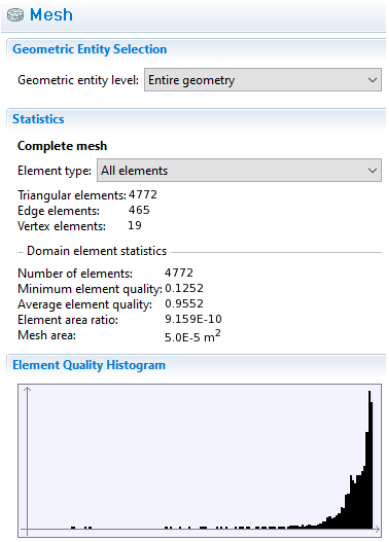

Figure 10. Applying the Mesh function

In Comsol Multiphysics, a study was achieved to determine the maximum unit stress up to which the specified material area does not fail, and the results are highlighted in figure 11. To determine the optimal value, the parameter tau0Fe2O3 (breaking strength of iron oxide) was varied.

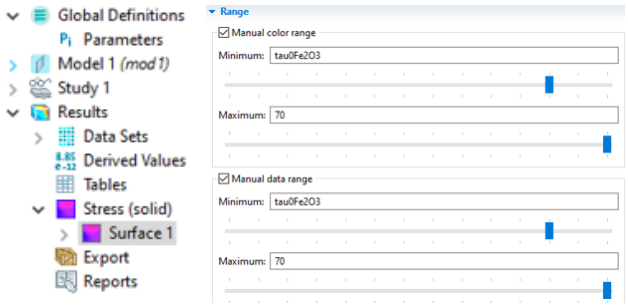

Figure 11. Defining the breaking strength of the depassivated material (iron oxide)

4. ANALYSIS OF THE ARRANGEMENT OF THE PASSIVATED LAYER

In figure 12, the area where ultrasonic depassivation occurs on the processed surface can be observed. The elements presented are the area of removed material, the base material of the analyzed model, and the microgeometry peak.

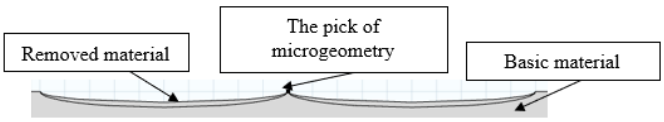

Figure 12. Highlighting the processed area

Figures 13-16 present the variations in the areas from which the material layer is removed and the arrangement of the passivated layer based on the applied ultrasonic cavitation pressure. The influence of ultrasonic cavitation pressure was analyzed starting from a value of 30 MPa. At an ultrasonic pressure of around 25-30 MPa, it can be observed that the layer removed from the base material is larger. This indicates that to achieve uniform machining with an emphasis on the removal of the passivated layer, the value of the ultrasonic cavitation pressure should be reduced.

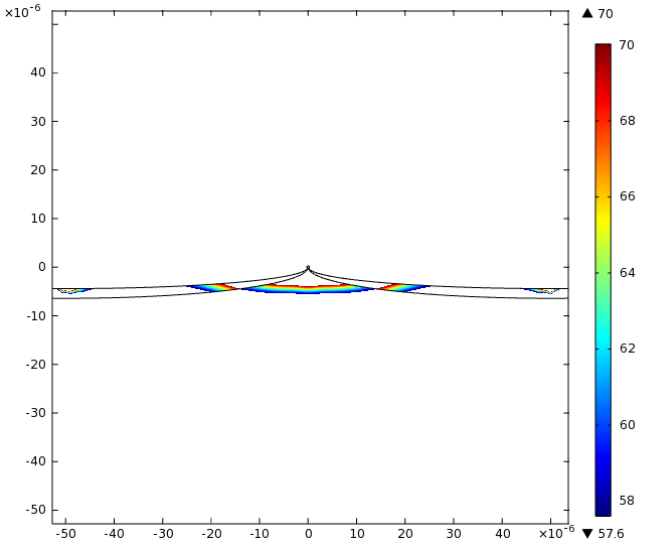

Figure 13. Arrangement of the passivated layer and the removed material layer, applied pressure = 30 MPa

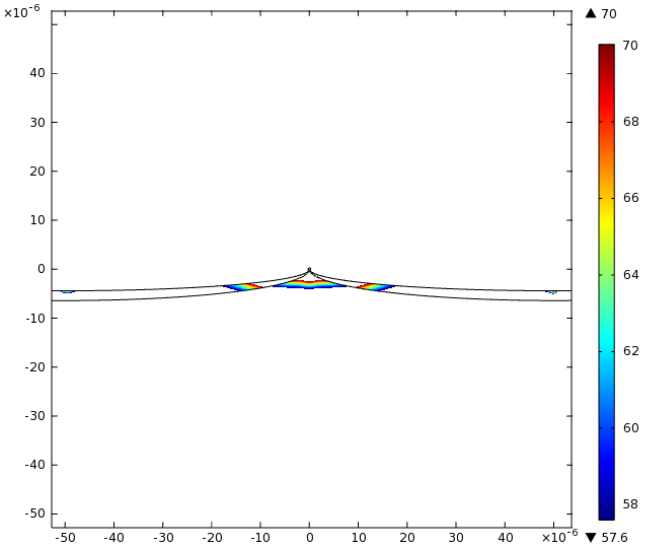

Figure 14. Arrangement of the passivated layer and the removed material layer, applied pressure = 25 MPa

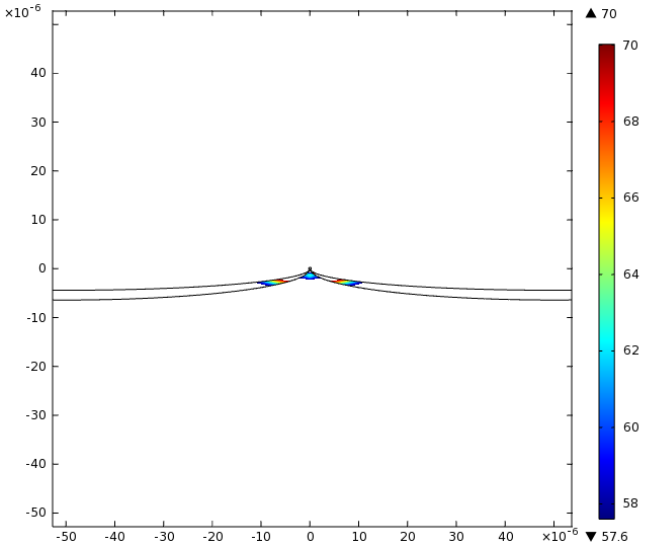

Figure 15. Arrangement of the passivated layer and the removed material layer, applied pressure = 20 MPa

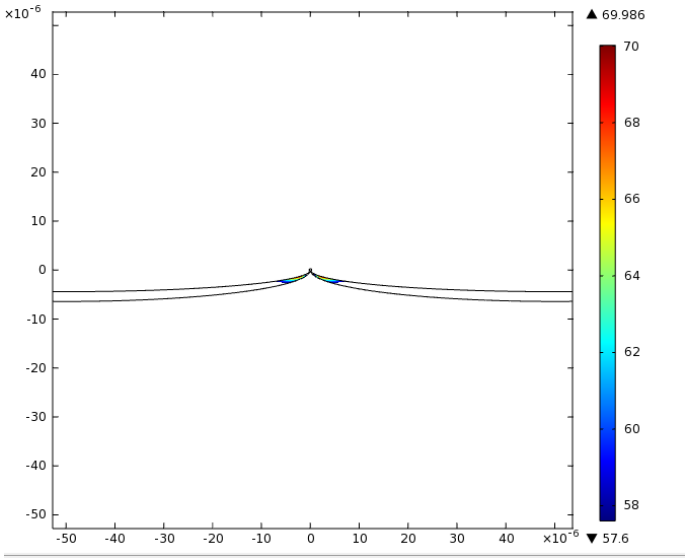

Figure 16. Arrangement of the passivated layer and the removed material layer, applied pressure = 17 MPa

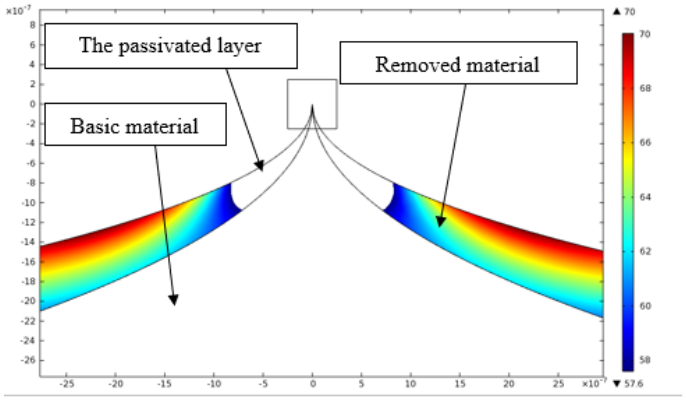

Figure 17. Distribution of unit stress during depassivation at applied pressure

It can be observed that at the applied pressure of 17 MPa (figure 16), determined from a study conducted on multiple models, only the passivated layer is removed.

The detailed 2D representation of the material eliminated through the combined action of ultrasonic cavitation and electrochemical machining is shown in figure 17. In this case, a relatively low ultrasonic cavitation pressure of 17 MPa was applied with the aim of removing the neutral layer (depassivation).

The area of the passivated layer can be observed in relation to the base material and the layer of material removed following the application of hybrid electrochemical-ultrasonic machining.

5. THE INFLUENCE OF VARIATIONS IN ULTRASONIC CAVITATION PRESSURE ON THE DEPASSIVATION OF IRON OXIDE

Table 1 presents the data obtained from Comsol Multiphysics for the graphical analysis of iron oxide depassivation.

Table 1. Iron oxide depassivation data

pus [MPa]	h_1 [µm]
17	2.6329
18	2.9934
19	3.2757
20	3.5251
21	3.7697
22	3.9728
23	4.1629
24	4.3391
25	4.4954
26	4.6448
27	4.7841
28	4.8857
29	5.0144
30	5.1168

The parameters mentioned in the table are:

h_1 - the depth of the passivated layer [µm]

pus - the ultrasonic cavitation pressure [MPa]

In figure 18 is presented the influence of ultrasonic cavitation pressure on the depassivation of iron oxide.

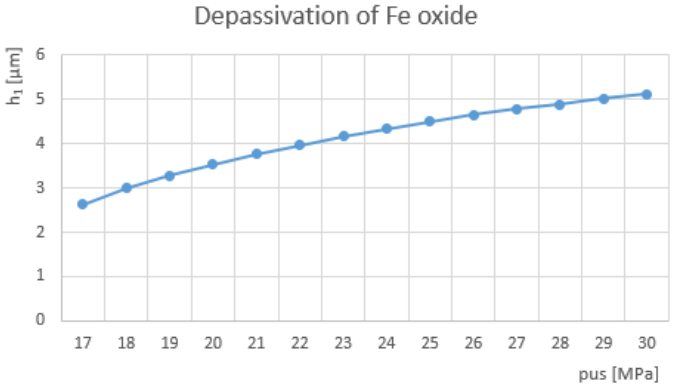

Figure 18. The influence of ultrasonic cavitation pressure on the depassivation of iron oxide

From the graphic representation, it can be concluded that a minimum ultrasonic cavitation pressure is required for depassivation, with an applied pressure of 17 MPa. At higher values, the removal of the base material occurs, which can lead to a reduction in roughness and productivity (rate of material removal). The modeling and simulation results were tested and validated through the development of the electrochemical-ultrasonic machining equipment shown in figure 19.

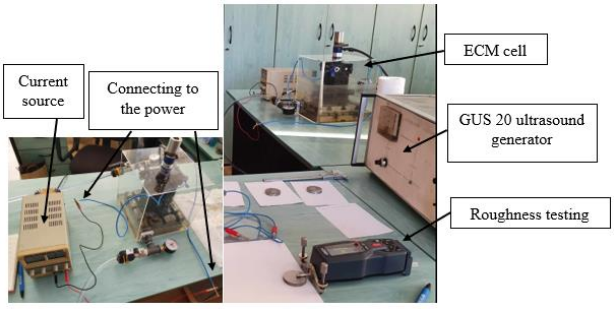

Figure 19. Hybrid finishing technological system ECM+US, experimental model [10]

Then figure 20 shows the architecture of the hybrid finishing equipment for electrochemical-ultrasonic machining, where the positioning of each component within the working system can be observed.

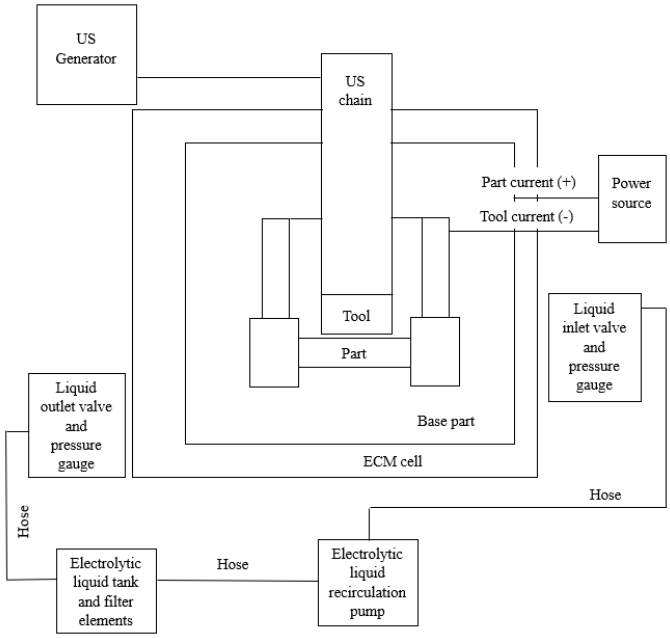

Figure 20. Hybrid finishing equipment architecture, electrochemical-ultrasonic machining [10]

6. CONCLUSIONS

A study was realised on several models in which the value of ultrasonic cavitation pressure was varied to determine the arrangement and volume of the removed material layer, with a C120 steel base structure. The influence of ultrasonic cavitation pressure on the depassivation of iron oxide, which occurs on the processed surface as a result of the electrolysis phenomenon in hybrid electrochemical-ultrasonic finishing, was studied. It was found that with the increase in ultrasonic pressure, the depth of the removed passivated layer also increases, and at pressures of at least 20 MPa, simulations from Comsol Multiphysics indicate that a layer of the base material is also removed starting from the micro-peak regions. This facilitates the surface finishing process and ensures uniform machining. Lower values of ultrasonic pressure, below 20 MPa, promote the depassivation process while also increasing productivity (rate of material removal).

After analyzing ultrasonic depassivation, specific to the hybrid electrochemical ultrasonic machining (ECM+US), the removal of the passivated iron oxide layer through the action of ultrasonic cavitation induced in the machining working gap, the next step in the research will focus on modeling the removal of microgeometry peaks on the processed surface and the decrease of roughness. In this phase, the applied load, the pressure exerted by ultrasonic-induced cavitation, will be in the range of hundreds of MPa.

7. REFERENCES

[1]. Hassan, E.H., *Vibration-assisted electrochemical machining: a review*, The International Journal of Advanced Manufacturing Technology, Vol. 105, p. 579-593, (2019).

[2]. Saxena, K.K., Qian, J., Reynaerts, D., *A review on process capabilities of electrochemical micromachining and its hybrid variants*, International Journal of Machine Tools and Manufacture, Vol. 127, p. 28-56, (2018).

[3]. Nicoara, D., Hedes, A., Sora, I., *Ultrasonic Enhancement of an Electrochemical Machining Process*, Proceedings of the 5th WSEAS International Conference on Applications of Electrical Engineering, Prague, Czech Republic, Vol. 5, p. 213-218, (2006).

[4]. Zhang, Y., *Investigation Into Current Efficiency For Pulse Electrochemical Machining Of Nickel Alloy*, Industrial and Management Systems Engineering, M.S. Thesis, University of Nebraska - Lincoln, (2010).

[5]. Katiyar, P.K., Randhawa, N. S., Hait, J., Jana, R.K., Singh, K.K., Mankhand, T.R., *Anodic Dissolution Behaviour of Tungsten Carbide Scraps in Ammoniacal Media*, In Advanced Materials Research, Vol. 828, p. 11-20, Trans Tech Publications, Ltd., (2013).

[6]. Reza, R.H., Mohammadreza, S., *Machining of 304 stainless steel Using Electrochemical Machining (ECM) Process: Response Surface Methodology Approach*, International Journal of Industrial Engineering & Production Research, Vol. 31, p. 397-407, (2020).

[7]. Kharche, W.G., Bilgi, D.S., Surekar, S.H., Bhatwadekar, S.G., *Depassivation Method of Hard Passive Alloys by Electrochemical Machining*, IOSR Journal of Mechanical and Civil Engineering (IOSR-JMCE), p. 42-45, (2012).

[8]. Drobota, V., *Rezistenta materialelor*, Editura tehnica, (1982).

[9]. Ghiculescu, D., *Chapter 5 - Ultrasonically Aided Electrical Discharge Machining, Manufacturing Technology Reasearch*, Electrical Discharge Machining - Types, Technologies and Applications, M.P. Jahan Editor, Nova Science Publishers, ISBN:978-1-63483-598-5, (2015).

[10]. Enciu, C.C., *Research on hybrid electrochemical-ultrasonic finishing machining*, Teză de doctorat, UNSTPB, (2024).